
**Application of oil-water discrimination technology in fractured reservoirs
by using the differences between fast and slow shear-wave**

Cong Luo^{1,2,3*}, Xiangyang Li^{1,2,4*}, Guangtan Huang^{1,2}

¹ State Key Laboratory of Petroleum Resources and Prospecting, China University of Petroleum, Beijing, 102249, China.

² CNPC Key Laboratory of Geophysical Prospecting, China University of Petroleum, Beijing, 102249, China.

³ Unconventional Oil and Gas Cooperative Innovation Center, China University of Petroleum, Beijing, 102249, China.

⁴ British Geological Survey, The Lyell Centre, Research Avenue South, Edinburgh EH14 4AP Scotland, UK.

*Corresponding Author: Cong Luo, Xiangyang Li

Tele: +8618618398853, +8618911226219

E-mail address: lishang0228@163.com, xy11962@hotmail.com

ABSTRACT

Oil-water discrimination is of great significance to design and adjust development project for oilfields. For fractured reservoir, based on anisotropic S-wave splitting information, it becomes possible to effectively solve such problem that the traditional longitudinal wave exploration is difficult to deal well with due to the similar bulk modulus and density of these two fluids. In this paper, by analyzing the anisotropic character of the Chapman (2009) model, the velocity and reflection coefficient differences between fast and slow S-wave caused by fluid substitution were verified. Then through wave field response analysis of the theoretical model, we found that water saturation causes larger time delay, larger time-delay gradient and lower amplitude difference between fast and slow S-wave, while the oil case is corresponding to lower time delay, lower gradient and higher amplitude difference. Therefore, a new class attribute was proposed, that is, the amplitude energy of the fast and slow shear wave, used for oil-water distinction. This new attribute and the time delay gradient attribute were both applied to the 3D3C seismic data of carbonate fractured reservoirs in the Luojia area of Shengli Oilfield in China. It shows that the prediction result of energy attribute has a better consistency with well information than time delay gradient attribute, and hence demonstrates the great advantages and potential of this new attribute in oil-water recognition.

Keywords: Oil and water discrimination; Chapman (2009) model; Seismic anisotropy; Fast and slow shear-wave

1 INTRODUCTION

Oil-water discrimination of reservoir has important implications for making and adjusting development plans of oil fields, and it is also the keystone and difficulty of oil exploration. From classical Gassmann formula, early geophysicists commonly believed that fluid information was inferred in P-wave data, with shear-wave being insensitive to fluid filled in rocks. So people focus more on using compression wave information to detect fluid (Quintal and Schmalholz et al 2010, Li 2012, Macbeth 2012, Quintal 2012, Zong and Yin 2015, Wu and Li 2015). The similar bulk moduli and densities of water and oil causes a weak effect on pure P-wave velocity and impedance under fluid substitution, and this impeded efforts to discriminate water and oil fluid types from conventional P-wave data analysis. However, it will encounter the seismic

anisotropy phenomenon when we study fractured rocks. For the fluid-filled fractured rocks, the rock physics relationships and wave field responses are different from the previous isotropic case.

Crampin (1977, 1978, 1981, 2005) found the shear-wave splitting phenomenon in monitoring nature earthquake: when a shear wave enters fractured rock, it splits into two quasi-shear waves with near orthogonal polarizations and different velocities, one with faster propagation velocity is called fast shear-wave and the other with slower velocity is called slow shear-wave. For a long time, researchers put emphasis on the link between shear-wave splitting attribute and fracture properties, and the shear-wave anisotropy was used to estimate fracture strike and some specific parameters (Crampin 2012, Quintal 2013, Verdon and Andreas 2013, Foord 2015). Along with the further research, it is found that the anisotropic information of rocks with fluid-filled fractures is closely related to the fluid properties. Schoenberg (1988) proposed a classical concept, the so called the excess compliance, which is associated with fracture network of rocks and can be expressed as the form of the sum of two parameters, the normal compliance (Z_N) and the tangential compliance (Z_T) of fractures. A typical assumption is that Z_N will vary with fluid bulk modulus whereas Z_T will be insensitive to fluid properties. Sayer (2015) pointed out that the normal compliance of a fluid-filled vertical fracture decreases with increasing fluid bulk modulus and the sensitivity of the S-wave splitting to fluid bulk modulus depends on the fracture interconnectivity, the background medium permeability and fluid saturation. Thomsen (1995) pointed out that, during seismic wave propagation, the fluid pressure gradient between fracture with high compliance and equant pore with high stiffness will force fluid to flow from fractures to pores, and such fluid substitution will strongly affect the anisotropic elastic properties of rocks. The fluid pressure variation of pore space will change the closure degree of compliant cracks and hence cause a change of the effective elastic constant of fractured rock, further varies the shear-wave splitting value (Zatsepin and Crampin, 1997). Based on Hudson's model, it shows that the ratio of normal to tangential compliance is related to the saturated fluid and it is possible to use seismic data to estimate fluid properties, theoretically at least (Liu and Li et al., 2000). Chapman and Maultzsch (2003) found out that due to fluid viscosity changing, the fluid substitution in reservoirs with fluid-filled micro-cracks and meso-fractures had a significant influence on the slow shear-wave. Because of fluid viscosity difference, slow S-wave can potentially give access to

fluid-saturation information in fractured rocks, even in circumstances in which the P-wave response is rather insensitive to fluid (Qian *et al.*, 2007). Through laboratory observation, Tillotson and Chapman (2010) proved that the S-wave splitting in synthetic rocks with penny-shaped fractures show significant changes with respect to fluid viscosity and fracture orientation. It means that fluids with different viscosities may be distinguished by S-wave information.

Although water and oil have similar velocities and densities, the viscosities of the two fluids often markedly different and it has been already mentioned that there is a connection between fluid viscosity and some kind of S-wave anisotropy of fractured rock. If we can determine this relationship and extract such anisotropic information from real seismic data we will greatly improve our chances to discriminate between these two fluids.

In this paper, based on Chapman (2009) fractured rock model, we offer a theoretical analysis of seismic anisotropy characteristics induced by fluid substitution. A certain connection between the difference between fast and slow shear-wave and fluid viscosity is discovered, and we present a new strategy for fluid discrimination, which is applied to 3D3C data from LuoJia area of Shengli oilfield in China. In research area, the carbonate reservoir containing high-angle fractures can be simplified as HTI media, so choosing Chapman (2009) model to analyze the anisotropic responses of fractured rock is reasonable.

2 SEISMIC ATTENUATION MECHANISM AND CHAPMAN MODEL

When a seismic wave passes by, slight deformation of rocks will occur and then produce stress and strain, further allow the seismic wave to propagate forward. For the case that meso-fractures, micro-cracks and micro-pores are all contained in rocks, pressure gradient due to seismic wave force will induce a fluid exchange between compliant fracture or crack and stiff equant pore, this process finally causes seismic wave dispersion and attenuation. Fluid flow helps stress to reach a new equilibrium. Because of the viscous effect of fluid-filled rocks, the stress relaxation and strain recovery are delayed. The time required to relax stress is called relaxation time and influenced by many properties. Higher porosity, larger fracture scale and higher fracture density usually increase rock permeability, and hence increase the amount of fluid that flows per unit time, finally decrease the time for fluid stress equilibrating. While

viscosity influences fluid flowing rate, fluid with higher viscosity moves slower and longer relaxation time is needed in equilibrium stress. For lower fluid mobility case, more relaxation time corresponding to lower seismic frequency is required to reach a new pressure balance. Therefore, seismic frequency, fluid viscosity, rock background medium properties, such as porosity, fracture scale and fracture density affect the process of fluid stress equilibrium caused by wave propagation, and thus impact on seismic properties like dispersion and attenuation. When using rock physics model to study seismic dispersion, attenuation and frequency-dependent anisotropy, we need to consider the mentioned factors above in order to describe the seismic attenuation mechanism more authentically.

Traditional techniques for modelling fractured rock make use of static equivalent medium theories in the long wavelength limit. Schoenberg's (1980) linear slip model and Hudson's (1981) isolated crack model both assume that cracks embedded in the isotropic elastic medium are fluid-isolated, without considering the influence of pores. Thomsen (1995) proposed the equant pore model consisting of a set of parallel cracks and randomly distributed equant pores to allow fluid to exchange between cracks and surrounding rock. However, only the exact expressions of anisotropic parameters and elastic compliance matrix in the low- and high-frequency limit were given. These models above are defined as static equivalent media models because they are used to describe rock elastic properties only in the case of low- and high-frequency limit. However, real seismic data from fractured reservoir show that seismic attenuation and dispersion, as well as anisotropic information are frequency-dependent (Parra, 2000; Van der Kolk et al., 2001; Maultzsch et al., 2007). Some extracted information from multicomponent data such as fast and slow shear-wave time delay varies with frequency (Liu et al., 2003; Maultzsch, 2003). Therefore, it is necessary to select dynamic equivalent media models, which can describe the elastic response of fractured rock in the whole frequency band.

The theories related to dynamic fracture model have also been developed. Hudson et al. (1996) improved and proposed a new equant pore model with considering the wave-induced fluid substitution between cracks and equant pores, but this model is not effective in the whole frequency band. Parra (2000) combined BISQ (Biot/Squirt flow theory) with Thomsen theory to establish rock model allowing fluid flow from cracks to pores, however, due to micro-cracks assumption, the dispersion and attenuation

estimates of this model are much lower than that in seismic frequency band. The effective-medium theory based on the work by O'Connell and Budiansky (1977) and by Sayer and Kachanov (1991) refers to as BOSK theory (Hudson and Crampin, 2003). The BOSK is also a dynamic equivalent model for describing velocity attenuation (Kolk et al., 2001), but the flow-induced attenuation and dispersion mechanism is not clear in this model (Hudson and Crampin, 2003). Chapman (2002) put forward a micro squirt flow model to simulate the fluid flow between micro crack and spherical pore. With the comprehensive analysis from micro to meso scales, Chapman (2003) built a rock model including spherical micro-pore, randomly distributed ellipsoidal micro-crack and a single set of parallel meso-fracture. When the wave-induced fluid pressure gradient exists in fractured rock, two-scale fluid flow are simulated in Chapman (2003) model, one is mesoscale fluid flow which occurs between meso-fractures and micro-cracks or pores, and the other is microscale fluid exchange from micro-cracks to micro-pores. In the low and high frequency limit, this model is respectively equivalent to the anisotropic Gassmann formula and Hudson's (1981) isolate crack model, which shows the validity of this model under condition of low and high frequency limit. Chapman (2003) model is limited to a single set of fractures. It is necessary to consider more complex fracture distribution within the model to fit for more geological realities (Barton, 2007). Retaining the advantages of Chapman (2003) model, Chapman (2009) extended earlier model (Chapman, 2003) to the case of multiple sets of fractures with different scales and orientations. Furthermore, in the calculation of elastic constants of rocks, the aforementioned factors that affect the rebalancing of wave-induced fluid pressure, including fluid properties, medium parameters and seismic wave frequency, are considered in this model. The Chapman (2009) model can make a reasonable explanation of seismic dispersion and attenuation and can be applied to study seismic frequency-dependent anisotropy of fluid substitution.

3 FLUID-INDUCED DIFFERENCE OF FAST AND SLOW SHEAR WAVE

The high-angle fractures in reservoirs can be approximately regarded as vertical ones. Based on Chapman (2009) theory, we build a theoretical model with a set of vertical fractures, equant pores and cracks, consider the fluid exchange between fractures or cracks and pores and analyze the fluid-induced anisotropic characteristics of velocity and attenuation.

3.1 Velocity difference

By using Chapman (2009) theory to calculate the equivalent elastic matrix of fractured rock model, phase velocities and attenuation from different azimuth angles and different propagation directions are obtained by solving the Christoffel equation. In figure 1, we plot the attenuation for qP -, qS - and S -wave three wave modes as a function of propagation angle, an angle of 0° corresponds to vertical and 90° is horizontal. The attenuation of both qP - and qS -wave is significant, with pure S -wave not being obviously attenuated. The reasons of this phenomenon are as follows. The polarization direction of fast shear-wave is perpendicular to its propagation direction, its vibration occurs in the vertical plane which is parallel to fractures, the fractures can hardly be compressed and little fluid flows between fractures and pore space, so little attenuation occurs. On the contrary, both qP - and qS -wave do compress the fractures, then the compression-induced fluid exchange causes the attenuation. Within the angle range (from 0° to 45°) typically concerned in reflection seismology, qS -wave has a greater effect of attenuation than qP -wave.

Chapman (2009) describes the microscopic and mesoscopic fluid flow types corresponding to two relaxation times. The relaxation time between micro cracks and pores is given by

$$\tau_m = \frac{c_v \eta (1 + \sigma_c / k_f)}{\sigma_c \kappa \zeta c_1} \quad (1)$$

where c_v is the volume of the individual crack, c_1 is the number of pores which a crack is connected to, ζ is the grain scale of background medium, $\sigma_c = \pi \mu r / [2(1 - \nu)]$ is supercritical pressure, η is fluid viscosity, k_f is fluid bulk modulus, ν is the Poisson's ratio of the matrix material and r is the aspect ratio of fractures and cracks. The fracture-related fluid pressure relaxation time is represented by a larger value τ_f

$$\tau_f = \frac{8\ell(1 - \nu)(1 + \sigma_c / k_f)}{3\mu} \left(\frac{\eta}{\kappa} \right) a_f \quad (2)$$

where κ is permeability and a_f is radius of fractures. It can be seen that both τ_m

and τ_f are proportional to the fluid viscosity. It means that the viscosity shows fluid flow velocity in rocks, fluid with higher viscosity flows slower and hence longer relaxation time is needed in equilibrium pressure. Only the fluid viscosity variation is considered while the other parameters remain the same, the high viscosity corresponds to the long relaxation time.

The stronger attenuation of slow S-wave (qS -wave) in typically concerned angle range (from 0° to 45°) may have many influencing factors. This time, we are more concerned about the fluid substitution effects. Figure 2 and 3 show the dispersion curves of qP -wave travelling perpendicular to fractures, fast (pure S-wave) and slow S-wave for two different viscosity corresponding to two relaxation time, with all wave modes propagating at 25° from vertical. The velocity of fast S-wave is not dispersed or affected by fluid viscosity. The velocities of both qP - and slow S-wave increase with frequency. With the relaxation time increasing, the dispersion curve of qP -wave moves towards higher frequency and that of slow S-wave shifts to lower frequency. While both of them create a frequency band in which the velocities are sensitive to fluid viscosity variation. Slow S-wave has a greater frequency-dependent change of velocity than qP -waves and suffers more attenuation.

In fact, though the bulk modulus and densities of oil and water are similar, but when comprehensively analyzing the frequency-dependent anisotropy induced by oil and water substitution, there are still slight differences which need to be considered. In figure 4, we show the dispersion curves of fast and slow S-wave for oil and water saturated conditions, when the propagation angle is 25° . Comparing to figure 3, the starting and ending velocities are slightly different because of fluid density and bulk modulus changing. However, the overall tendencies of curves are basically same, which also demonstrates that fluid viscosity is the primary cause of dispersion difference of slow S-wave.

Figure 5 demonstrates the percentage curves of S-wave splitting decrease with non-dimension frequency for oil and water saturation. The S-wave splitting is used to describe the velocity difference between fast and slow S-wave and is defined as $100(V_{S1} - V_{S2})/V_{S1}$, where V_{S1} and V_{S2} are velocities of fast and slow S-wave respectively. The S-wave splitting curve of oil saturation decreases rapidly in the range

of less than 1Hz, while, for the water-saturated case, percentage value changes within the range of 1-100Hz. From this figure, it is obvious that S-wave splitting value is sensitive to oil-water substitution. Within the seismic frequency band (from 1Hz to 100Hz), water saturation gives rise to higher percentage of S-wave splitting corresponding to higher velocity difference value than the oil-saturated case. Hence, it can be inferred that the time delay between fast and slow S-wave for water saturation is longer because that the larger difference of seismic velocity causes the larger difference of travel time. In theory, from actual fast and slow S-wave data, it may be possible to mining fluid information of fractured reservoir.

3.2 Reflection coefficient difference

Besides travelling time, the actual seismic signals also contain a wealth of information of amplitude, frequency, phase and other components that are also likely to hide fluid information. The differences of the reflection coefficients of PP- and PS-wave between the fracture parallel and fracture normal directions can be written as below (Li, 1998)

$$\Delta R_{PP} = \frac{1}{2} \left[\delta_2 - \delta_1 - 2\varepsilon_2 + 2\varepsilon_1 + \frac{8V_{S0}^2}{V_{P0}^2} (\gamma_2 - \gamma_1) \right] \sin^2 i \quad (3)$$

$$\begin{aligned} \Delta R_{PS} = & \frac{\sin i}{2 \cos j} \left[\frac{V_{P0}^2}{V_{P0}^2 - V_{S0}^2} (\delta_2 - \delta_1 - 2\varepsilon_2 + 2\varepsilon_1) + \frac{4V_{S0}^2}{V_{P0}^2} (\gamma_2 - \gamma_1) \cos i \cos j \right. \\ & - \frac{V_{P0}V_{S0}}{V_{P0}^2 - V_{S0}^2} (\delta_2 - \delta_1 - 2\varepsilon_2 + 2\varepsilon_1) \cos i \cos j - \frac{4V_{S0}^2}{V_{P0}^2} (\gamma_2 - \gamma_1) \sin^2 i + \\ & \left. (\delta_2 - \delta_1 - 2\varepsilon_2 + 2\varepsilon_1) \sin^2 i - \frac{V_{P0}^2}{V_{P0}^2 - V_{S0}^2} (3\delta_2 - 3\delta_1 - 4\varepsilon_2 + 4\varepsilon_1) \sin^2 i \right] \quad (4) \end{aligned}$$

where, i and j are the average propagation angles of the upper and lower medium for the reflected PP- and PS-wave respectively, V_{P0} and V_{S0} are the average background P- and S-wave velocities of the upper and lower medium. $\delta_k, \varepsilon_k, \gamma_k$ ($k = 1, 2$) are the Thomsen anisotropic parameters for the upper ($k = 1$) and lower ($k = 2$) medium.

Figure 6 shows the variation of the calculated ΔR_{PP} and ΔR_{PS} with non-dimensional relaxation time. The reflection coefficient differences of both two wave

modes increase with increasing relaxation time. Yet the gradient of ΔR_{pS} is larger than that of ΔR_{pP} , which means that ΔR_{pS} is much more sensitive to variation of relaxation time, that is to say it is sensitive to fluid viscosity.

4 THEORETICAL MODEL TEST

Based on the comprehensive study of various kinds of data in LuoJia research area, including preliminary geological data, well logging data and drilling core data, a three-layer fluid saturated pore-fracture rock model was established. The carbonate reservoir of the first member of Shahejie Formation in study area is our target layer that has mesoscale high angle fractures, and hence it can be simplified as HTI medium with vertical fractures. The overburden layer is thick mudstone and the lower layer is fine sandstone, and both of them are set as isotropic media in the model. The background medium properties are derived from well logging curves, as shown in table 3. Fractures and dissolved pores are developed in the target stratum and the fluids in reservoir space are oil and water, the property parameters of reservoir space and fluid are sourced from drilling core data and laboratory measurement results, as shown in table 1 and table 2. The depth of the target layer is 1000m in the model, the offset range is set as 0-1200m, and the maximum wave propagation angle is about 31° . We used Chapman (2009) theory to calculate the elastic matrix of the middle fractured layer, and adopted the reflectivity forward modelling method to simulate the multicomponent wave field.

Figure 7 and 8 are synthetic multicomponent seismograms for water- and oil-saturated cases, respectively. In both of two figures, a and b are the vertical and radial components for propagation parallel to fracture strike, c and d are the vertical and radial components for propagation perpendicular to fracture strike. When fractured layer is saturated by water, the zero offset travelling time t_0 of reflected S-wave from bottom interface of fractured layer are 1221ms and 1230ms in the parallel and perpendicular fracture direction, while, for the oil case, t_0 corresponding to bottom interface S-wave reflection in parallel and perpendicular fracture direction are 1224ms and 1247ms. The travelling time in the direction of parallel fracture strike is obviously shorter than that of perpendicular fracture strike. So when propagation is parallel to fracture the fast S-wave field is obtained, and the synthetic record of perpendicular direction is the slow

S-wave field, which is consistent with our theoretical understanding.

4.1 Time delay difference

In order to observe the travelling time difference in different azimuth (time-delay) more intuitively, we calculate the correlation values of the obtained vertical and radial components in parallel and perpendicular fracture direction. Figure 9 and figure 10 respectively show the time delay spectra of reflected P-and S-wave, the X coordinate of solid triangle corresponds to the time-delay value picked up in different time depth. The change of fluid properties causes no significant change of P-wave travelling time, the delay time of P-wave for water and oil saturated cases are both close to zero and the curves' tendency are similar, as shown in figure 9. However, for S-wave reflections, the result changes. In figure 10, the time-delay corresponding to the top interface of fractured layer is close to zero and does not obviously vary with fluid, while fluid substitution has an influence on the bottom interface reflection delay time which is no longer near-zero, and the maximum delay time for water saturation is 21.35ms is longer than that for oil case 8.58ms. Therefore, the delay time of bottom interface between fast and slow S-wave for water saturation is longer than that of the oil case, and the gradient of water-saturated time-delay curve is higher than that of the oil.

4.2 Amplitude difference

It has been concluded in 3.2 that the reflection coefficient difference of converted wave ΔR_{ps} between parallel and perpendicular fracture directions is sensitive to fluid viscosity, so it is speculated that the amplitude information of fast and slow S-wave records may contain fluid details. In order to quantitatively describe the amplitude variation in the synthetic records, we calculated and compared the RMS amplitudes of reflections from the top interface of fractured layer for water and oil saturation, shown as in figure 11. Figure 11a and 11b are the RMS amplitude curves of PP-wave reflection for oil and water saturation, the reflected energy of PP-wave is affected little by fracture azimuth and fluid substitution. Figure 11c and 11d show the corresponding reflected PS-wave behavior, the effect of fluid substitution on fast S-wave amplitude is weak. However, fluid change can cause amplitude energy difference of slow S-wave and this difference increases with offset increasing. The reason is that fast S-wave is unaffected by fluid viscosity and its slight difference is induced by fluid density and bulk modulus

changing, while fluid viscosity has clear impact on slow S-wave and fluid substitution induces obvious amplitude difference of slow S-wave.

In the figure 11, it is worth noting that, when rock model is saturated with water, the calculated amplitude values and curve trends of fast and slow S-wave are similar, while for oil case there are significant differences in amplitude and tendency. Then we calculated the reflection amplitude difference and ratio of top interface reflection of fracture layer of parallel and perpendicular fracture directions, as shown in figure 12. 12a and 12b are respective amplitude difference and ratio values of PP-wave reflection, and 12c and 12d are amplitude difference and ratio values of fast and slow S-wave. The amplitude differences and ratios of PP-wave are insensitive to fluid. While, the difference and ratio values of fast and slow S-wave for oil saturation are obvious larger than that for water case, the great difference between oil and water illustrates the high fluid sensitivity of amplitude difference and amplitude ratio attributes.

5 PRACTICAL APPLICATION

Through the previous analysis, we find that there are time-delay gradient difference and amplitude difference between oil saturation and water saturation in the theoretical fractured model. We propose to use the time-delay gradient and amplitude difference attributes of fast and slow S-wave to discriminate oil and water in the actual multicomponent data of LuoJia area of Shengli Oilfield in China.

LuoJia area is located in the South of Zhanhua depression in Bohai Bay basin. It has eight proven oil blocks, which shows a great potential for oil exploration. In this research, the target layer is Es1 fractured carbonate reservoir, the carbonate rocks in the first member of Es1 consist of bio-clastic limestones, sandy-clastic rocks and dolomites and so on. Intergranular dissolved pores, intragranular dissolved pore and high-angle fractures in the carbonate rocks increase reservoir porosity and permeability. By comparing the logging response characteristics of oil reservoir section and that of water ones in research area, we found that the reservoir section shows high P-wave velocity, high density, high resistivity, low gamma and low spontaneous potential logging response characteristics. There is no obvious difference between oil and water in logging response, so conventional attributes are insensitive to oil and water discrimination and new method is needed now.

5.1 Time delay attribute

According to the converted wave data in Luojia area, after determining the S-wave splitting angle, fast and slow S-wave data are obtained from the radial and vertical component data by rotating S-wave splitting angle. Based on the sliding-window correlative analysis of fast and slow S-wave, the S-wave time-delay spectrums of seismic traces near the oil well L971 and the water well L972 are calculated, which are used to analyze the delay time difference induced by fluid substitution, as shown in figure 13. In the figure 13, T2 and T6 correspond to the top and bottom interface of fractured reservoir respectively, and different colors denote different degrees of correlation. For well L971, the ES1 fractured reservoir with 55.3% oil saturation and 10455t cumulative oil production is a typical oil producing section, while the water saturation of ES1 section in well L972 is about 99.6% and the daily water production of this section is 14.7t. The figure 13a shows that the minimum and maximum delay time of target reservoir in L971 oil-production well is about 12.26ms and 19.7ms, the maximum time-delay difference is 7.48ms, and the curve gradient of picked-up time-delay with time depth (the curve of solid triangle) is small. The minimum and maximum delay time of L972 is about 11.48ms and 43.74ms, the maximum time-delay difference is 32.26ms, and the curve gradient is obviously larger than that of oil well L971. This phenomenon is in agreement with the former theoretical analysis and model test results and shows an obvious difference in time-delay curve gradients between water and oil saturation. Therefore, we calculated the time-delay gradient attribute to highlight fluid difference as shown in figure 14, and the colors mean the gradient values. The figure shows that the position saturated with water corresponds larger gradient, while the gradient of oil position is relatively lower. So time-delay gradient attribute of fast and slow shear wave can be used to distinguish oil and water, and better highlight the water bearing area.

5.2 Amplitude attribute

Based on the theoretical analysis in 4.2, we selected four oil-production wells L37, L944, L964, L966 and four water-production wells L66, L109, L92, L94 in the Luojia research area, and extracted traces near boreholes from fast and slow S-wave data to calculate the corresponding amplitude energy difference and ratio curves, as the figure 16 and 17 show. By intersection analysis of amplitude energy curves and conventional

logging curves of fractured reservoir section, the parameters sensitive to oil-water discrimination are optimized, and then the interpretation templates of cross plot are established. Figure 16a and 16b are the intersection results of P-velocity, respectively, with amplitude energy difference and ratio values of four selected water wells. Figure 17a and 17b are the intersection results by using data of four oil wells. It can be seen that the target section of water wells is manifested as the characteristics of lower P-velocity, lower energy differences and lower energy ratio, where the energy difference is less than 80 and the ratio value is less than 2. The oil reservoir corresponds to the characteristics of higher P-velocity, higher energy differences and higher energy ratio, where the energy difference is greater than 80 and the ratio value is greater than 2. There is an overlapping area of P-velocities between oil and water, which hinders the oil-water distinction by using P-velocity. However, the energy difference and ratio between fast and slow S-wave data can clearly distinguish oil and water in the cross-plots.

Based on the feasibility analysis of well data, the identification of oil and water is carried out in seismic data. Figure 18 and 19 show the energy attributes of fast and slow S-wave across water well L66 and oil well L37, respectively. Figure 18a and 19a are both energy difference attribute profiles, 18b and 19b are the energy ratio profiles. In the figure 18, the energy difference and ratio values near water well L66 are respectively less than 80 and 2, while the energy differences and ratios near oil well L37 in figure 19 are obvious high values in the range of 80-350 and 2-6.2, respectively. The high difference and ratio values indicate oil area, these results consistent with well-data intersection analysis. Figure 20a and 20b are the energy difference and ratio attribute sections of well-tie line, the black dashed lines represent the locations of the water wells and the red dashed lines are the oil-well locations. The prediction results of these two attributes are in good agreement with the well information. In order to monitor the prediction accuracy, we calculated the correlation degree of the attribute predicted results and the well information. The prediction accuracy of the energy difference attribute is about 71.5%, and the accuracy of the energy ratio prediction reaches 83.33%, all these demonstrate the feasibility of oil-water discrimination by energy difference and ratio attributes, and the latter one has a relatively higher

prediction accuracy.

By comparing the time-delay gradient and the amplitude energy attributes, we have got the following understandings.

Time-delay gradient between fast and slow S-wave can be used to distinguish oil and water, the oil region has low gradient value, and the water area is characterized by higher gradient and more prominent. However, there are some limitations in this method. First, the computation of delay time has a high requirement on the resolution and signal-noise ratio (SNR) of seismic data, lower resolution and SNR will reduce the credibility of the picked-up delay time. Second, because it is difficult to determine the specific range of the time delay gradient of oil and water saturation cases, this kind of attribute cannot be used for quantitative oil-water recognition at present.

It is feasible to use the amplitude energy attribute of fast and slow S-wave to distinguish oil and water, which has been proved by theoretical analysis, model test and practical data application above. The water-saturated area corresponds to lower energy difference and lower energy ratio, while the oil region has higher difference and higher ratio values and is more prominent. The results of this method has a better consistency with well information and a lower reliance on SNR and resolution of data. In addition, the value ranges of the two attributes of oil and water can be obtained by logging data intersection analysis that makes quantitative oil-water discrimination possible.

6 CONCLUSIONS

For anisotropic fractured reservoir, the fast and slow shear wave field contains important fluid information. Wave-induced fluid flow only causes slow S-wave attenuation without affecting the fast shear wave. Slow shear wave is sensitive to fluid viscosity, while fast S-wave does not vary with the viscosity of fluid. Fluid viscosity change causes obvious difference in S-wave splitting, hence induces time-delay difference between oil and water saturation, further cause time-delay gradient variation. In addition, the obvious viscosity difference of oil and water can also cause a change of

the amplitude difference between fast and slow S-wave, and the energy difference is lower value when fractured reservoir is saturated with water, while the oil bearing area is corresponding to the high energy difference. We then put forward a new class attribute, that is, the amplitude energy of fast and slow S-wave, for oil-water discrimination.

The new attribute and the time-delay gradient are applied to practical data and the results are analyzed and compared. The time-delay gradient attribute can highlight the water-saturated zone, but is easy to be impacted by SNR and resolution of seismic data and difficult to distinguish quantitatively. While the energy attribute gives prominence to the oil zone, and has a better consistency with well information and a lower reliance on processing effect of seismic data. These demonstrate that the amplitude energy attributes of fast and slow S-wave have a greater advantage and potential than time-delay gradient, and hence this kind of attribute is recommended for oil-water discrimination in practical application.

ACKNOWLEDGMENTS

The authors would like to thank Associated Editor and anonymous reviewers for their helpful comments, and also acknowledge the Shengli Oilfield Company for the donation of the data. This study is sponsored by National Natural Science Foundation of China (No.4147096 and No.U1262208).

REFERENCE

Barton, N., 2007, Rock quality, seismic velocity, attenuation and anisotropy: Taylor and Francis.

Chapman M., Zatsepin S.V. and Crampin S. 2002. Derivation of a microstructural poroelastic model. *Geophysical Journal International*, 151, 427–451.

Chapman, M., 2003. Frequency dependent anisotropy due to meso-scale fractures in the presence of equant porosity. *Geophysical prospecting*, 51, 369-379.

Chapman, M., Maultzsch S., Liu E. and Li X.-Y. 2003. The effect of fluid saturation in an anisotropic multi-scale equant porosity model. *Journal of Applied Geophysics*, 54, 191–202.

Chapman M., 2009. Modeling the effect of multiple sets of mesoscale fractures in porous rock on frequency-dependent anisotropy. *Geophysics*, 74, 97-103.

Crampin, S., King, D.W. 1977. Evidence for anisotropy in the upper mantle beneath Eurasia from the polarization of higher mode seismic surface waves. *Geophys. J. R. Astron. Soc.*, 49, 59-85.

Crampin, S., 1978. Seismic-wave propagation through a cracked solid: polarization as a possible dilatancy diagnostic, *Geophys. J. R. Astron. Soc.*, 53, 467-496.

Crampin, S., 1981. A review of wave motion in anisotropic and cracked elastic media. *Wave Motion*, 3, 343-391.

Crampin, S. and Peacock, S. 2005. A review of Shear-wave splitting in the compliant crack-critical anisotropic Earth. *Wave motion*, 41, 59-77.

Crampin, S., 2012. Evaluation of anisotropy by shear-wave splitting. *Geophysics*, 50(1):142-152.

Foord G., Verdon J., and Kendall J. 2015. Seismic characterization of fracture compliance in the field using P- and S-wave sources. *Geophysical Journal International*, 203(3):1727-1737.

Hudson, J. A., 1980. The excitation and propagation of elastic waves. Cambridge University Press.

Hudson, J.A., 1981. Wave speeds and attenuation of elastic waves in material containing cracks. *Geophysical Journal Royal Astronaut Society*, 64, 133-150.

Hudson, J.A., Liu, E. and Crampin, S., 1996. The mechanical properties of materials with interconnected cracks and pores. *Geophysical Journal International*, 124, 105-112.

Hudson, J.A. and Crampin, S., 2003. Comment on: 'The 3D shear experiment over the Natih field in Oman: The effect of fracture-filling fluids on shear propagation by C.M. van der Kolk, W.S. Guest and J.H.H.M. Potters. *Geophysical prospecting*, 51, 365-368.

Li X.-Y. 1998b. Processing PP and PS waves in multicomponent sea-floor data for azimuthal anisotropy: theory and overview. *Proceedings of the Eighth International Workshop on seismic Anisotropy (Revue De L'institut francia du petrole)*, 53, 607-620.

Liu, E., Li, X.-Y. and Queen J. H., 2000. Discrimination of porefluids from P and converted shear-wave AVO analysis. *Anisotropy 2000: Fracture, converted waves and case studies*, Soc. of Expl. Geophys.

Liu, E., Maultzsch, S., Chapman, M., Li, X.-Y., Queen, J.H. and Zhang, Z., 2003. Frequency-dependent seismic anisotropy and its implication for estimating fracture size in low porosity reservoirs. *The leading Edge*, 22, 663-665.

Li, Y. 2012. Gas reservoir identification by seismic AVO attributes on fluid substitution. *Applied Geophysics*, 9(2):139-148.

Macbeth, C. 2012. Azimuthal variation in P-wave signatures due to fluid flow. *Geophysics*, 64(4):1181-1192.

Maultzsch, S., Chapman, M., Liu, E. and Li, X.-Y., 2003. Modelling frequency-dependent seismic anisotropy in fluid-saturated rock with aligned fractures: implication of fracture size estimation from anisotropic measurements. *Geophysical Prospecting*, 51, 381-392.

Maultzsch, S., Chapman, M., Liu, E., et al. Modelling and analysis of attenuation anisotropy in multi-azimuth VSP data from the Clair field. *Geophysical Prospecting*, 2007, 55, 627-642.

Markov, G., Mukerji, T. and Dvorkin, J., 1998. *The rock physics handbook*, Cambridge university press.

Parra, J. O., 2000. Poroelastic model to relate seismic wave attenuation and dispersion to permeability anisotropy. *Geophysics*, 65, 202-210.

Pointer, T., Liu, E. and Hudson, J.A., 2000. Seismic wave propagation in cracked porous media. *Geophysical Journal International*, 142, 199-231.

Qian, Z., Chapman M., Li, X.Y., 2007. Use of multicomponent seismic data for oil-water discrimination in fractured reservoirs. *The Leading edge*, 26, 1176-1184.

Quintal, B., 2010. Schmalholz S, Podladchikov Y. Impact of fluid saturation on the reflection coefficient of a poroelastic layer. *Geophysics*, 76(2):N1-N12.

Quintal, B., Jänicke, R. and Rubino, J., 2014. Steeb H and Holliger K. Sensitivity of S-wave attenuation to the connectivity of fractures in fluid-saturated rocks. *Geophysics*, 79(5):WB15-WB24.

Quintal, B., 2012. Frequency-dependent attenuation as a potential indicator of oil saturation. *Journal of Applied Geophysics*, 82(7):119-128.

Sayer, C. M., 2015. Fluid-dependent shear-wave splitting in fractured media. *Geophysical prospecting*, 50(4):393-401.

Schoenberg, M., 1980. Elastic wave behaviour across linear slip interfaces. *Journal of the Acoustical Society of America*, 68, 1516-1521.

Schoenberg, M. and Douma, J., 1988. Elastic wave propagation in media with parallel fractures and aligned cracks. *Geophysical Prospecting*, 36, 571-590.

Thomsen, L. 1986. Weak elastic anisotropy. *Geophysics*, 51, 1954-1966.

Thomsen, L., 1995. Elastic anisotropy due to aligned cracks in porous rock. *Geophysical prospecting*, 43, 805-829.

Tillotson, P., Chapman, M., Best, A. et al., 2011. Observations of fluid-dependent shear-wave splitting in synthetic porous rocks with aligned penny-shaped fractures. *Geophysical Prospecting*, 59(1): 111-119.

Van der Kolk C.M., Guest W.S. and Potters J.H.H.M. 2001. The 3D shear experiment over the Natih field in Oman: the effect of fracture-filling fluids on shear propagation. *Geophysical Prospecting*, 49, 179–197.

Verdon, J., Andreas, W., 2013. Measurement of the normal/tangential fracture

compliance ratio (Z_N/Z_T) during hydraulic fracture stimulation using S-wave splitting data. *Geophysical Prospecting*, 61(s1):461-475.

Wu, X., Chapman, M., Li, X. and Boston, P., 2015. Quantitative gas saturation estimation by frequency-dependent amplitude-versus-offset analysis. *Geophysical Prospecting*, 62(6):1224-1237.

Zatsepin S.V. and Crampin S. 1997. Modelling the compliance of crustal rock—I. Response of shear-wave splitting to differential stress. *Geophysical Journal International*, 129, 477–494.

Zong, Z., Yin, X., Wu, G. and Wu, Z., 2015. Elastic inverse scattering for fluid variation with time-lapse seismic data. *Geophysics*, 80(2):WA61-WA67.

TABLES

Table 1. Properties of fracture, crack and pore

Fracture density(%)	Fracture aspect ratio	Fracture radius(m)	Crack aspect ratio	Porosity(%)
10	0.001	1	0.001	9.8

Table 2. Fluid properties

Fluid	Vp(m/s)	Density(g/cm ³)	Viscosity(Pas)
Water	1700	1.1	5×10^{-4}
Oil	1200	0.8	2×10^{-2}

Table 3. Background medium properties

Layer	Vp(m/s)	Vs(m/s)	Density(g/cm ³)	Thickness(m)
First	2700	1300	2.246	1000
Second	3490	1930	2.326	100
Third	3100	1700	2.265	Half-space

FIGURES

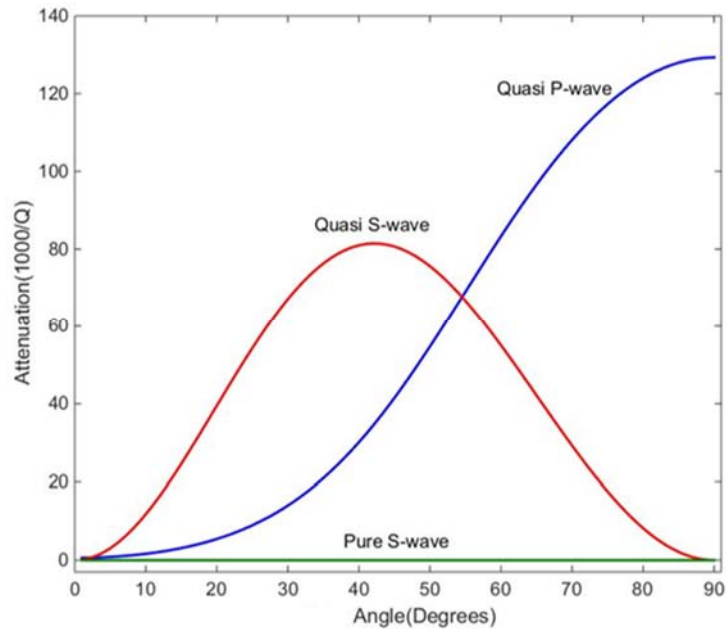


Fig. 1. Angular variation of calculated attenuation for qP -, qS - and S -wave three wave modes for a frequency of 30Hz and fracture size of 1m, an angle of 0° corresponds to vertical and 90° is horizontal.

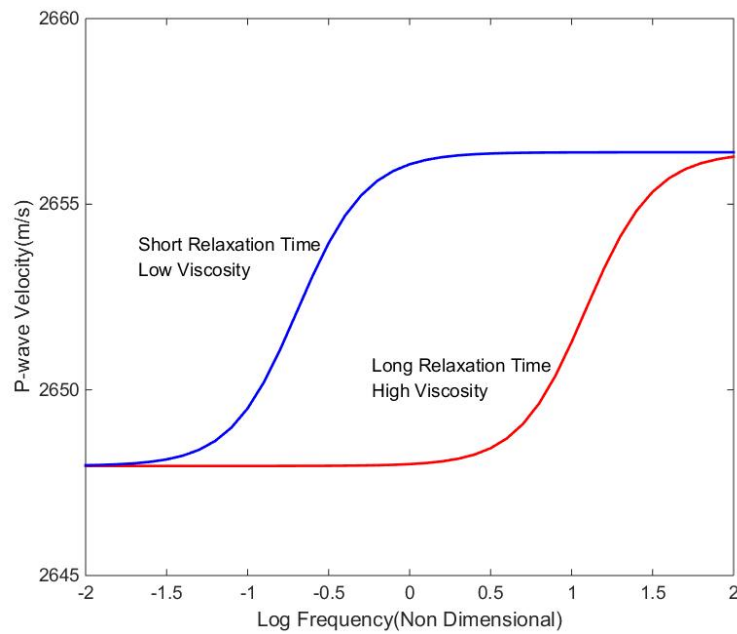


Fig. 2 Dispersion curves for qP -wave travelling perpendicular to the fractures, for two different relaxation time, with an angle of 25° .

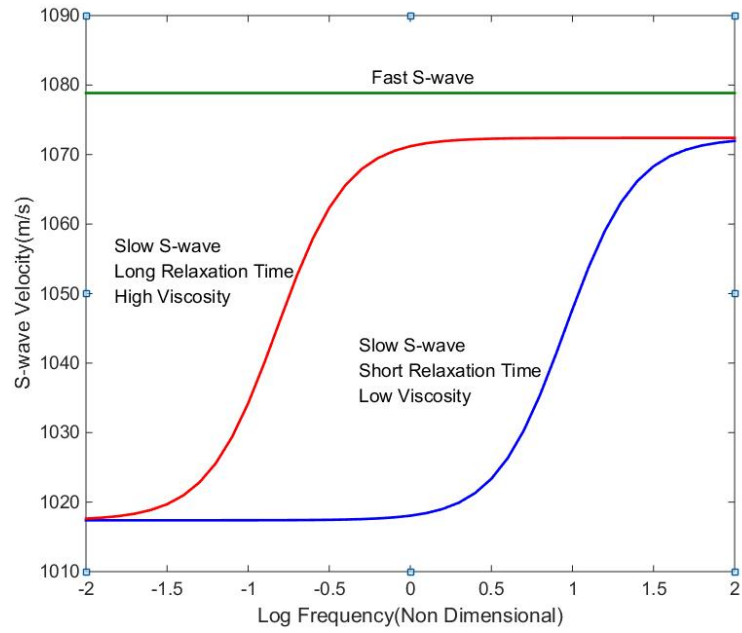


Fig. 3 Dispersion curves for fast and slow S-wave, for two different relaxation time, with an angle of 25° .

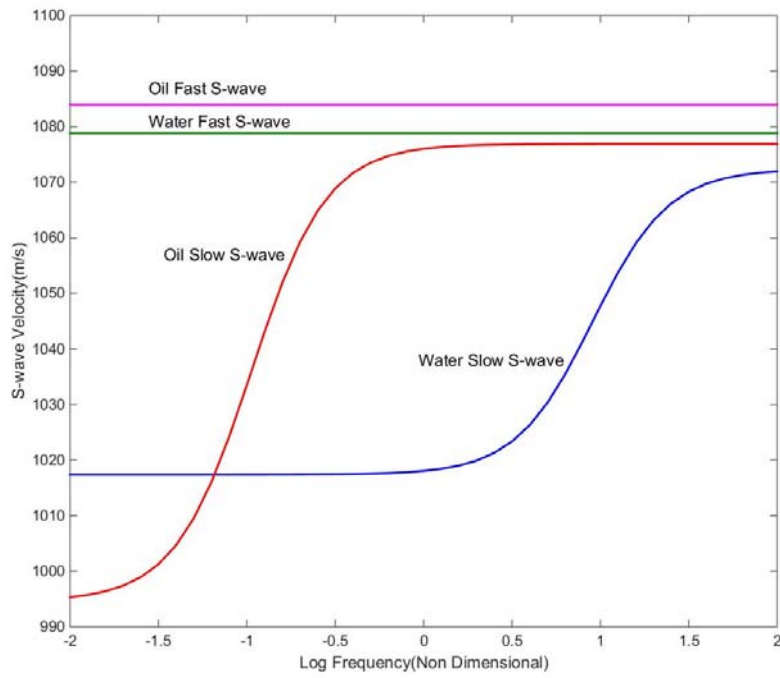


Fig. 4 Dispersion curves for fast and slow S-wave, for oil and water saturation, with a propagation angle of 25° .

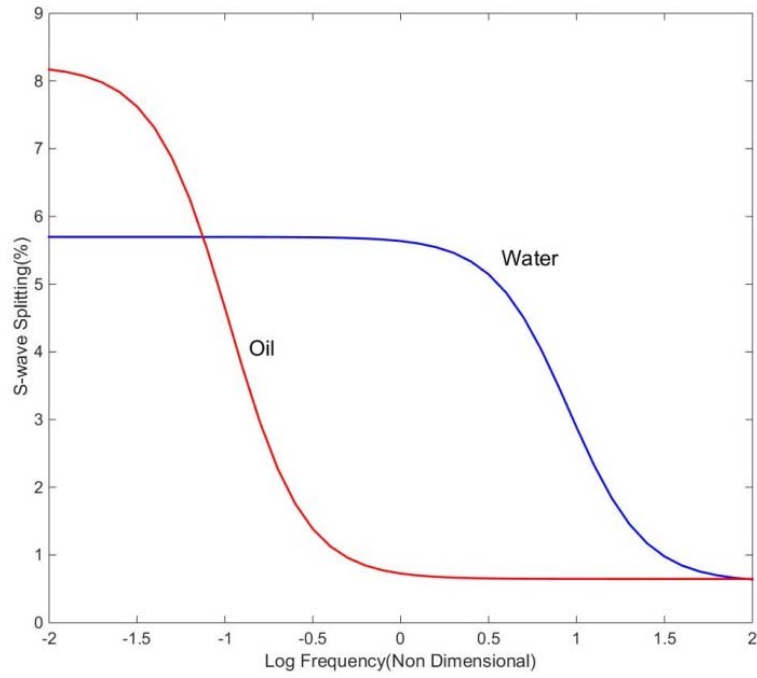


Fig. 5 The percentage value of S-wave splitting varies with non-dimensional frequency for oil and water saturation, with a propagation angle of 25° .

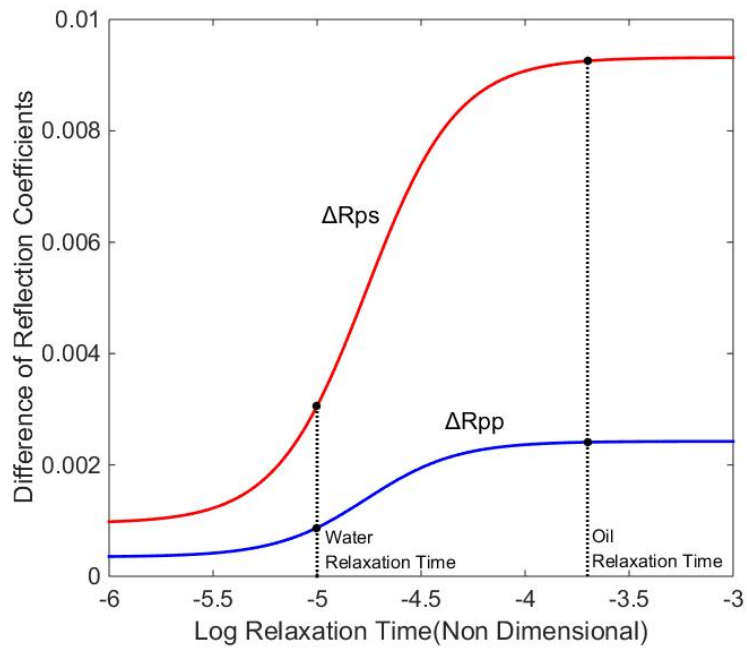


Fig. 6 The differences of the PP- and PS- wave reflection coefficients with non-dimensional relaxation time between the fracture parallel and fracture normal directions.

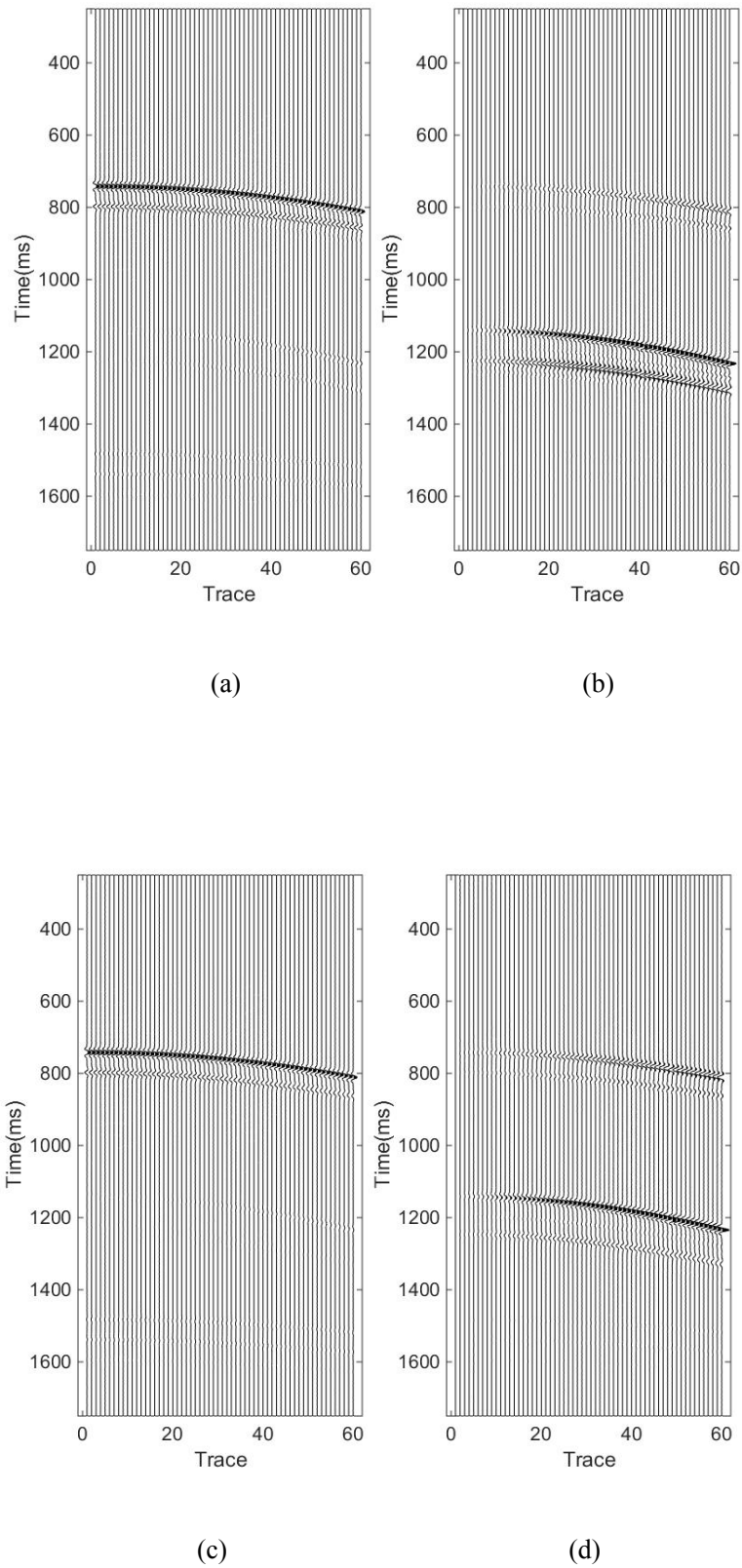
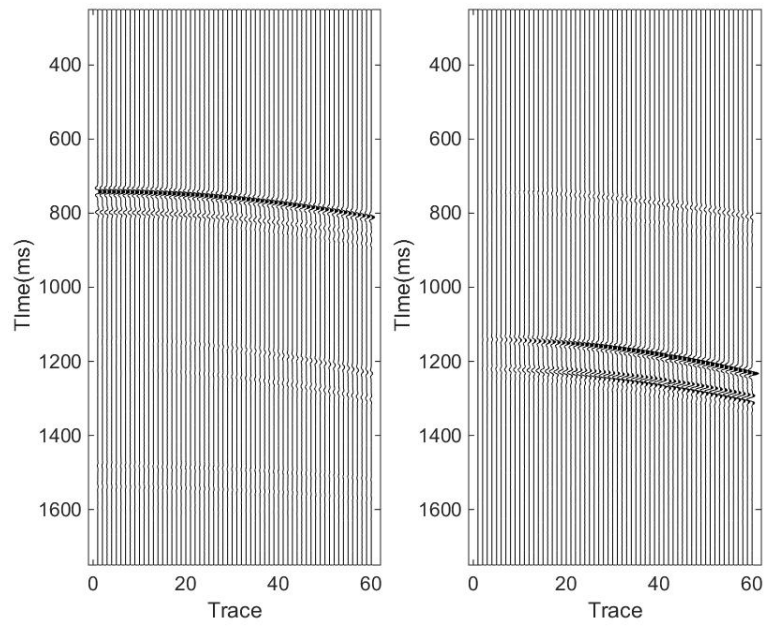
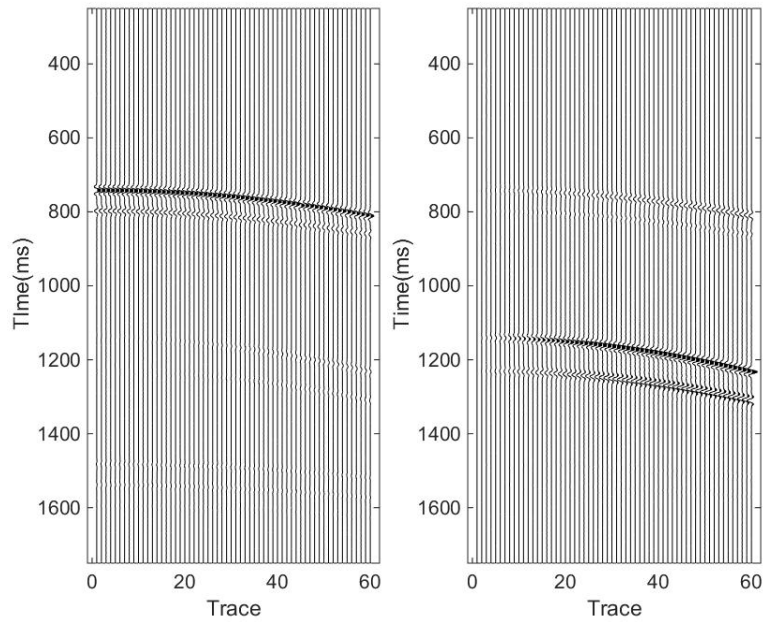


Fig. 7 The vertical (a, c) and radial (b, c) components of single shot synthetic seismograms for the three-layer water-saturated fractured model, propagation is parallel (a, b) and perpendicular (c, d) to fractures.



(a)

(b)



(c)

(d)

Fig. 8 The vertical (a, c) and radial (b, c) components of single shot synthetic seismograms for the three-layer oil-saturated fractured model, propagation is parallel (a, b) and perpendicular (c, d) to fractures.

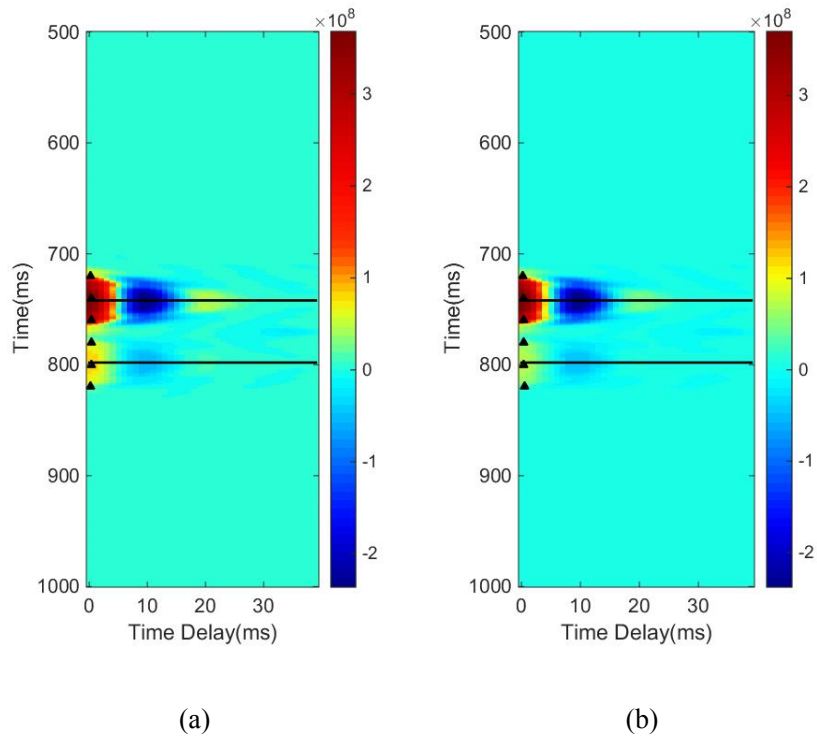


Fig. 9 P-wave reflection time-delay spectra of vertical components for water (a) and oil (b) saturation

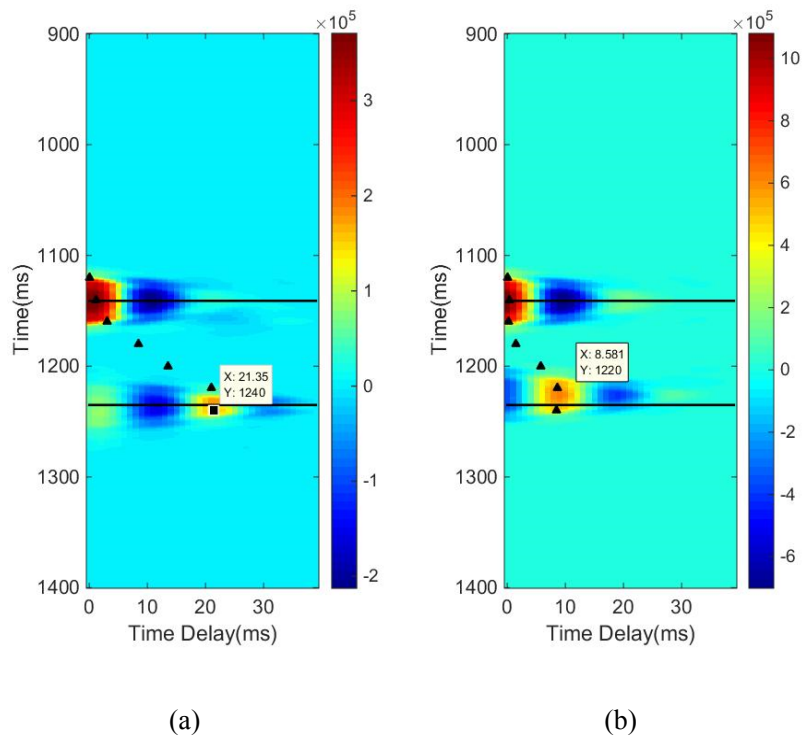


Fig. 10 Fast and slow S-wave time-delay spectra of radial

components for water (a) and oil (b) saturation

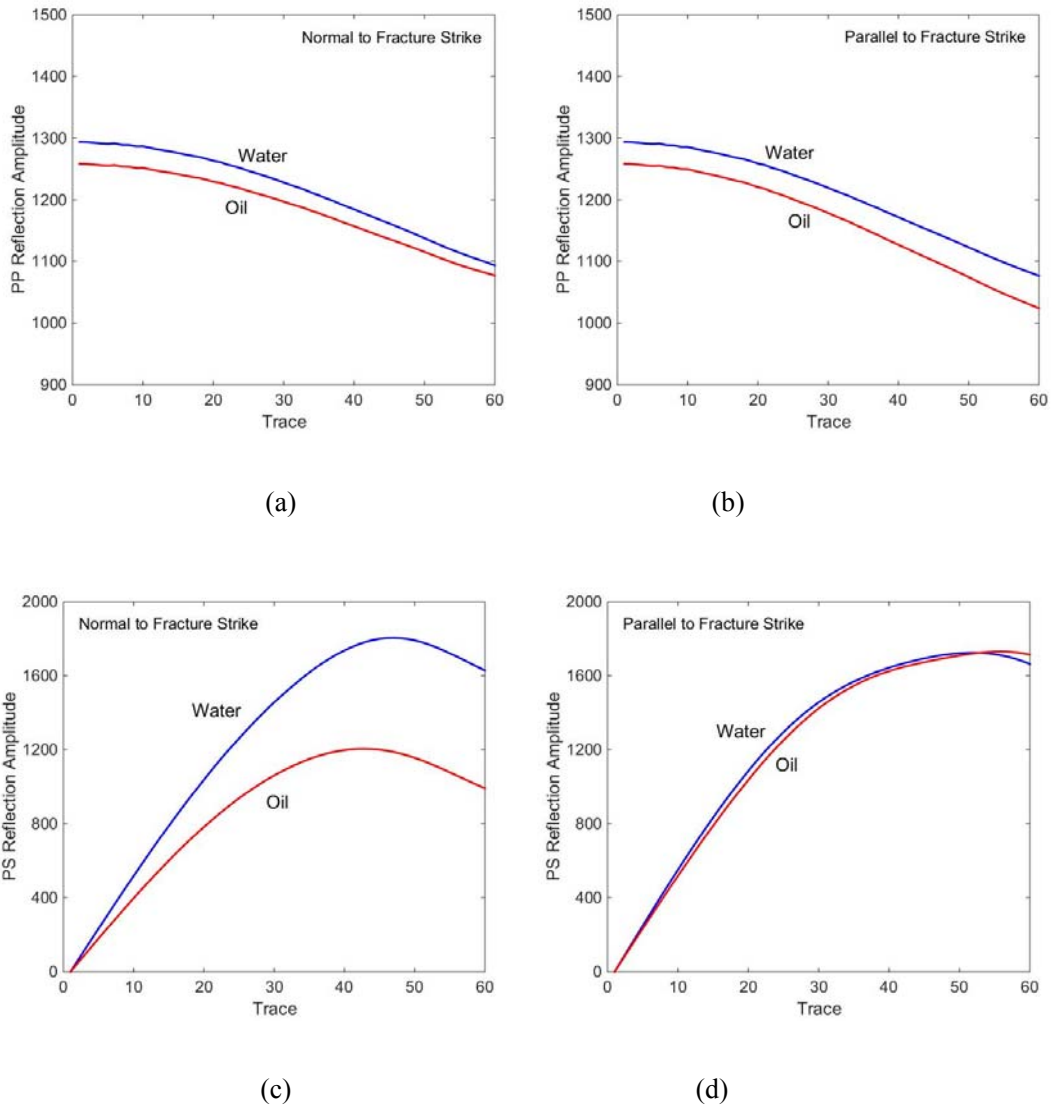
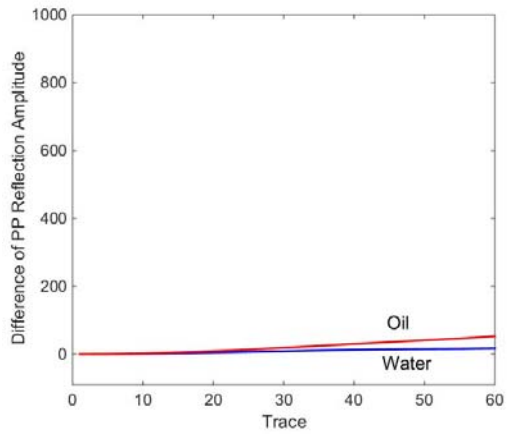
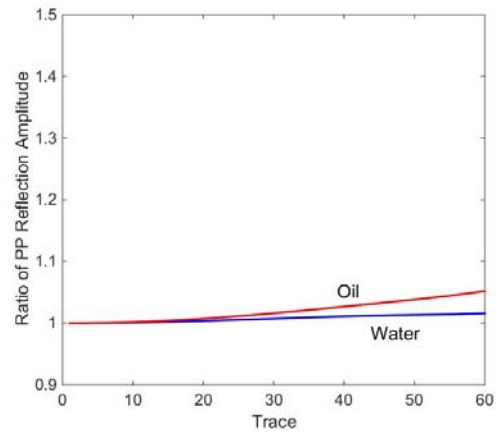


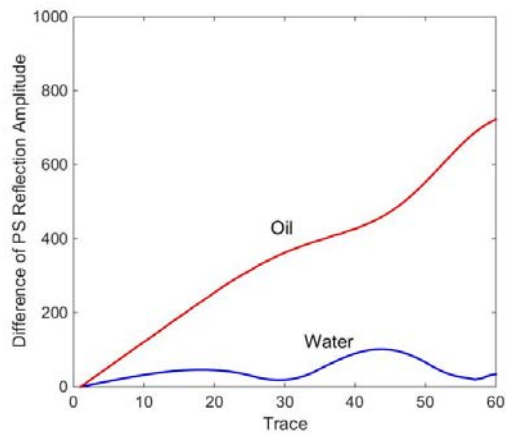
Fig. 11 The calculated RMS amplitudes of reflected PP- (a, b) and PS- (c, d) for propagation perpendicular (a, c) and parallel (b, d) to fracture strike for oil and water saturation.



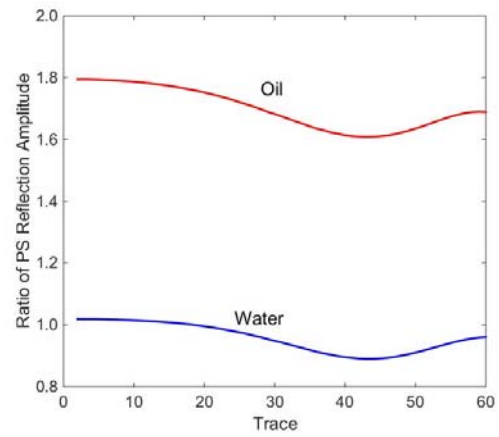
(a)



(b)



(c)



(d)

Fig. 12 The differences (a, c) and ratio (b, d) of PP- (a, b) and PS- (c, d) wave reflected from the top interface of fracture layer between perpendicular and parallel fracture directions.

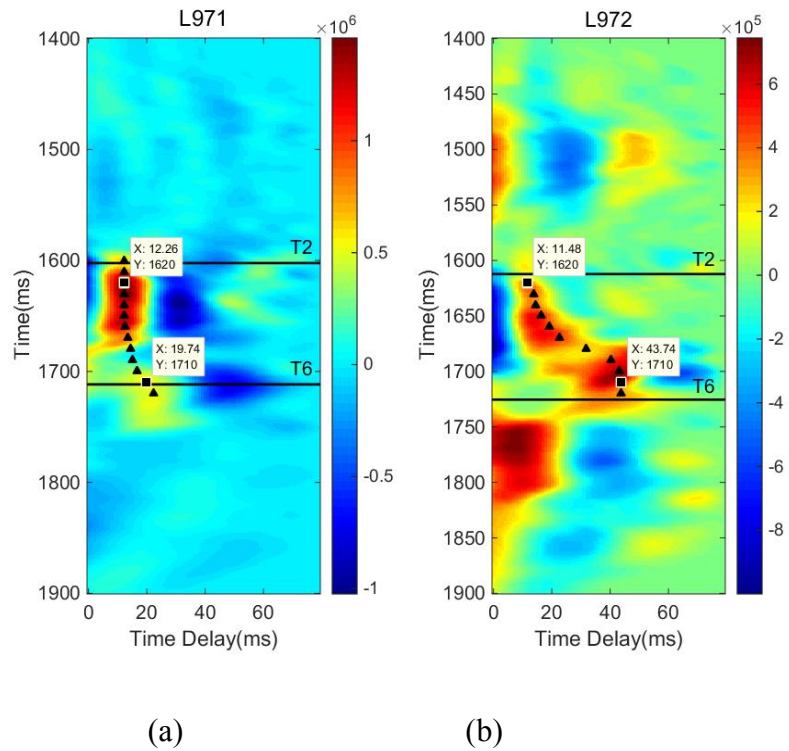


Fig. 13 The time-delay spectrum of fast and slow shear wave traces near the oil well L971(a) and the water well L972 (b), T2 and T6 correspond to the top and bottom interface of fractured reservoir, respectively, and the solid triangles are corresponding the picked-up time-delay values, different colors denote different degree of correlation.

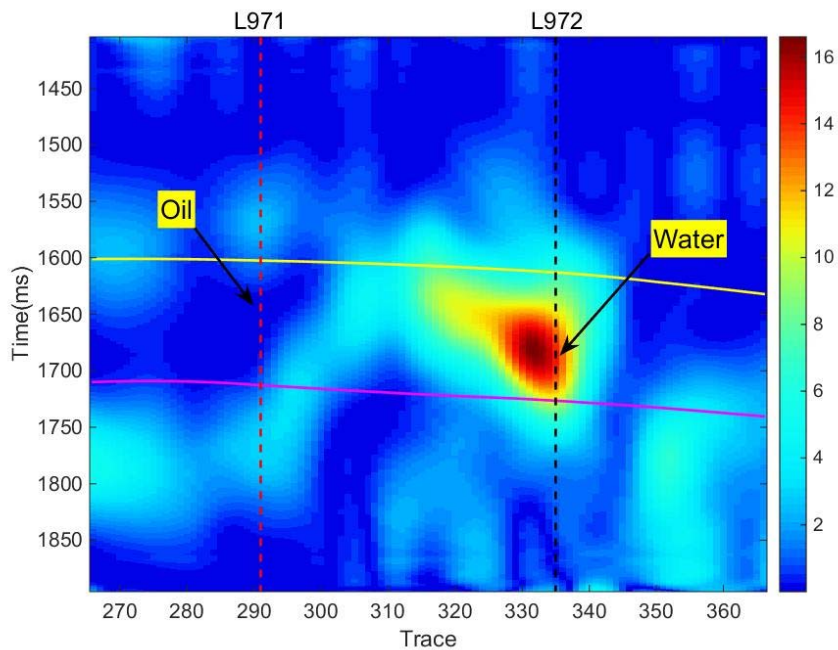
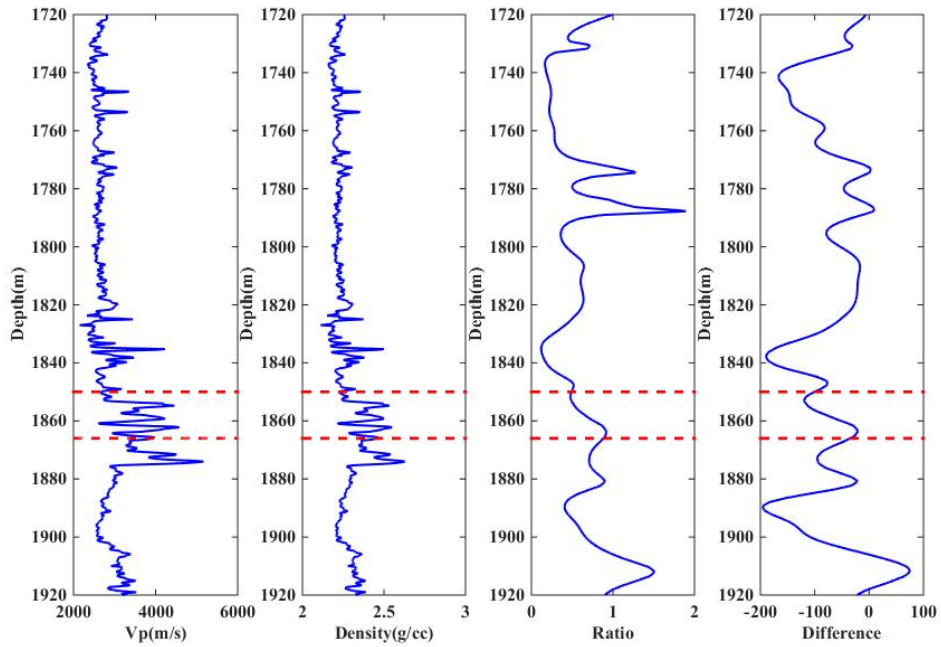
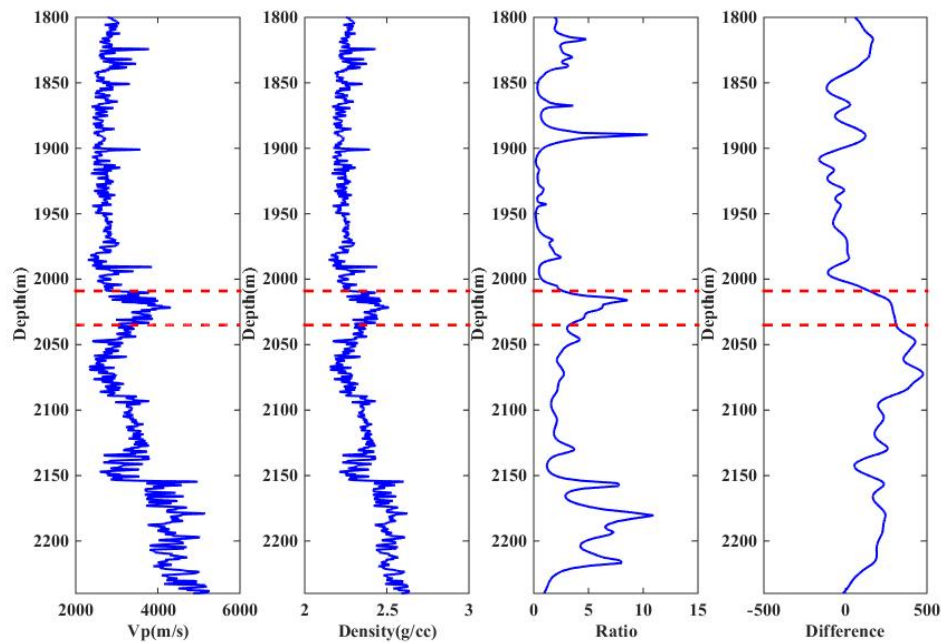


Fig. 14 The time-delay gradient section calculated by picked-up time-delay value, T2

and T6 correspond to the top and bottom interface of fractured reservoir, the colors mean the gradient values, the red and black dotted lines represent the locations of oil and water wells.



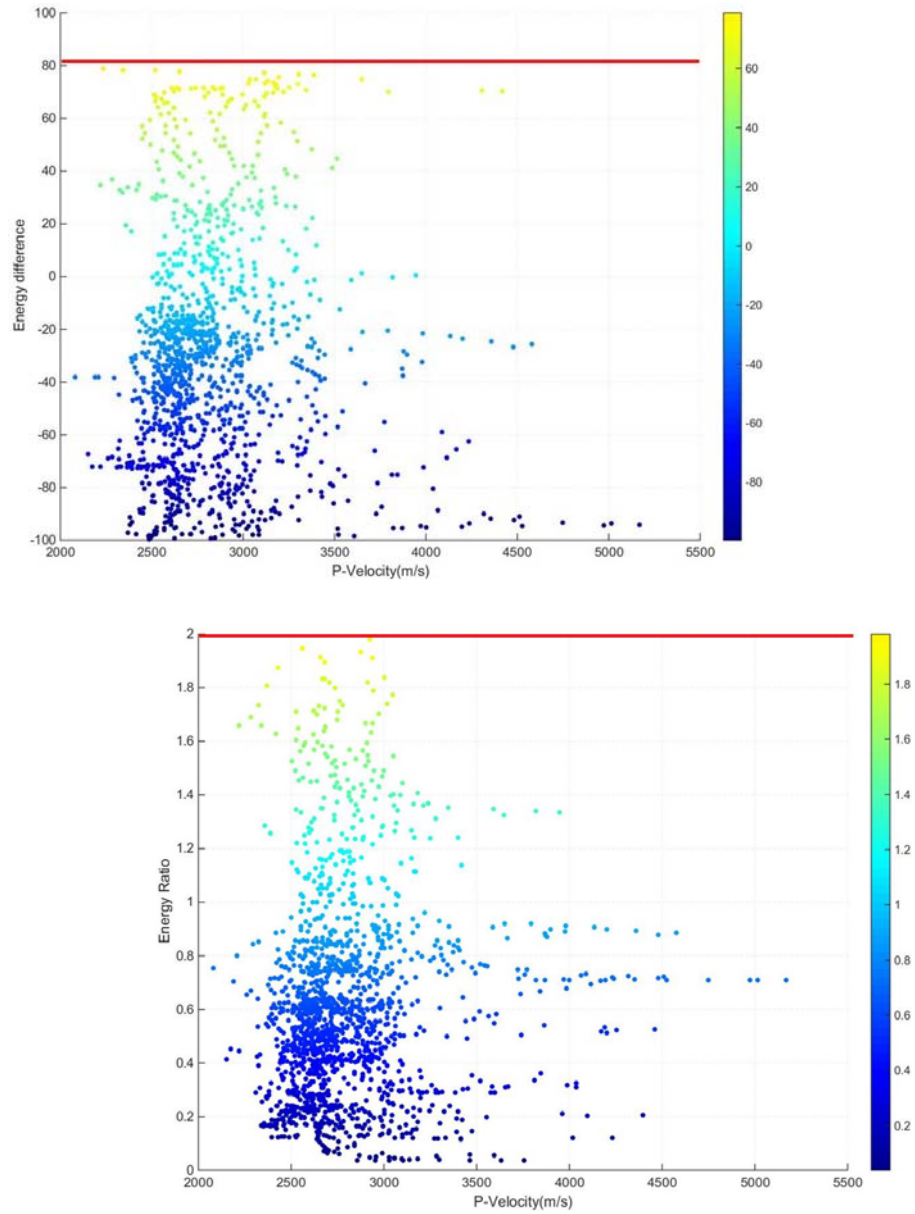
(a)



(b)

Fig 15. The well data of water well L94 (a) and oil production well L966 (b) including

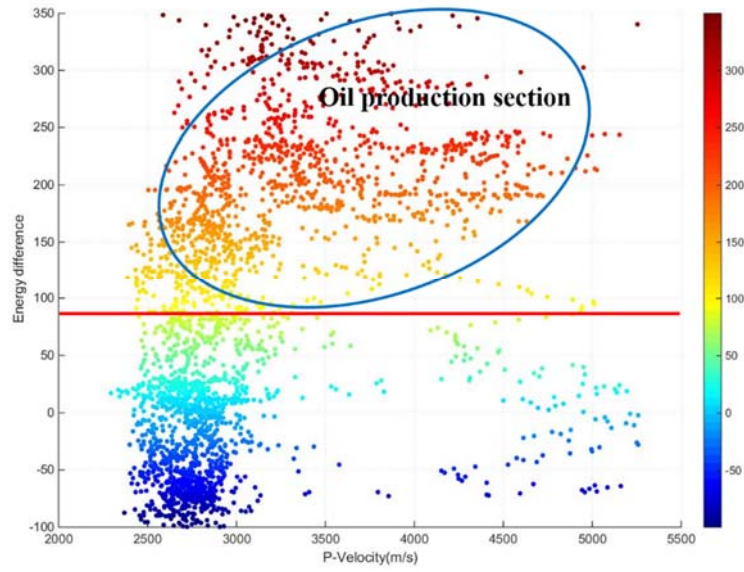
P-velocity, density, energy ratio and energy difference curve, where the energy ratio and difference values are calculated by fast and slow S-wave traces near the boreholes, and the red dotted lines represent the top and bottom interfaces of the reservoir.



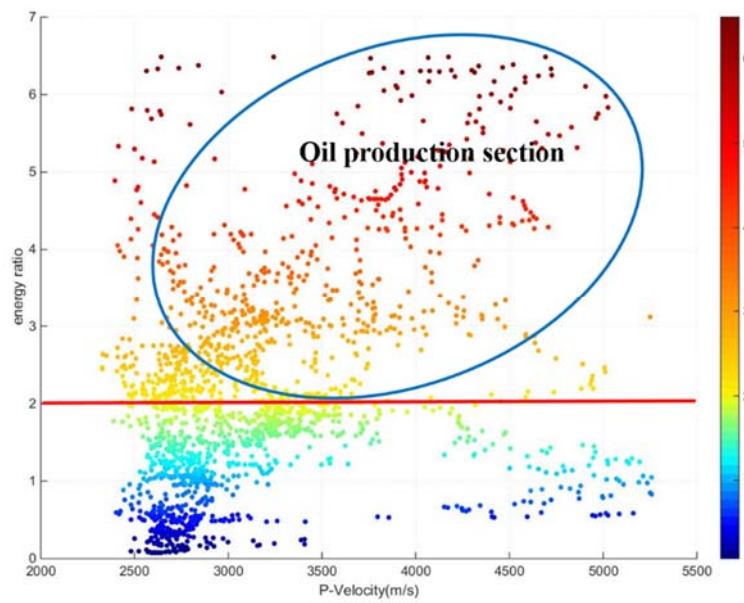
(a)

(b)

Fig. 16 the cross-plots of P-velocity with energy difference (a) and ratio (b) of the water wells L66, L109, L92 and L94, the colors represent the energy difference (a) and ratio values (b).



(a)



(b)

Fig. 17 The cross-plots of P-velocity with energy difference (a) and ratio (b) of the oil wells L37, L944, L964 and L966, the colors represent the energy difference (a) and ratio values (b).

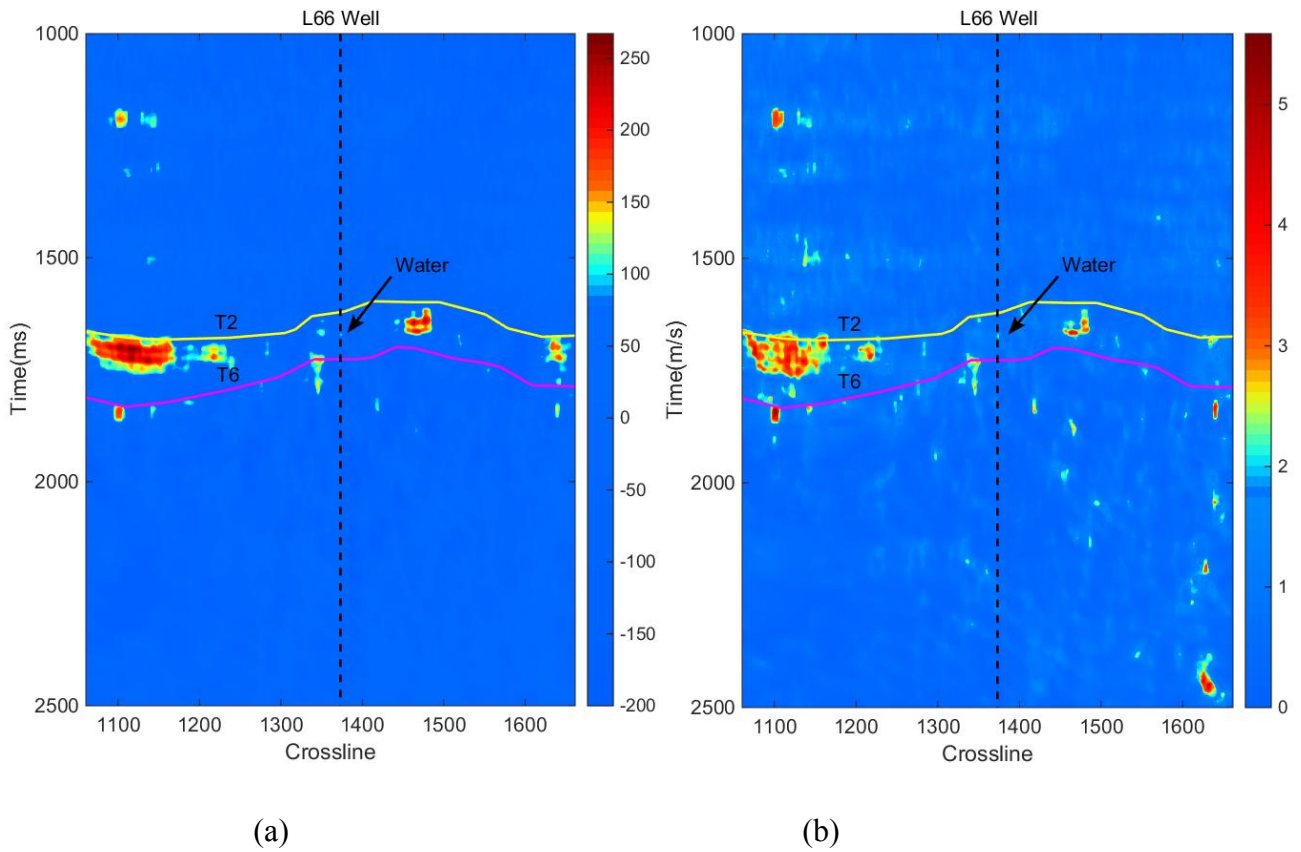
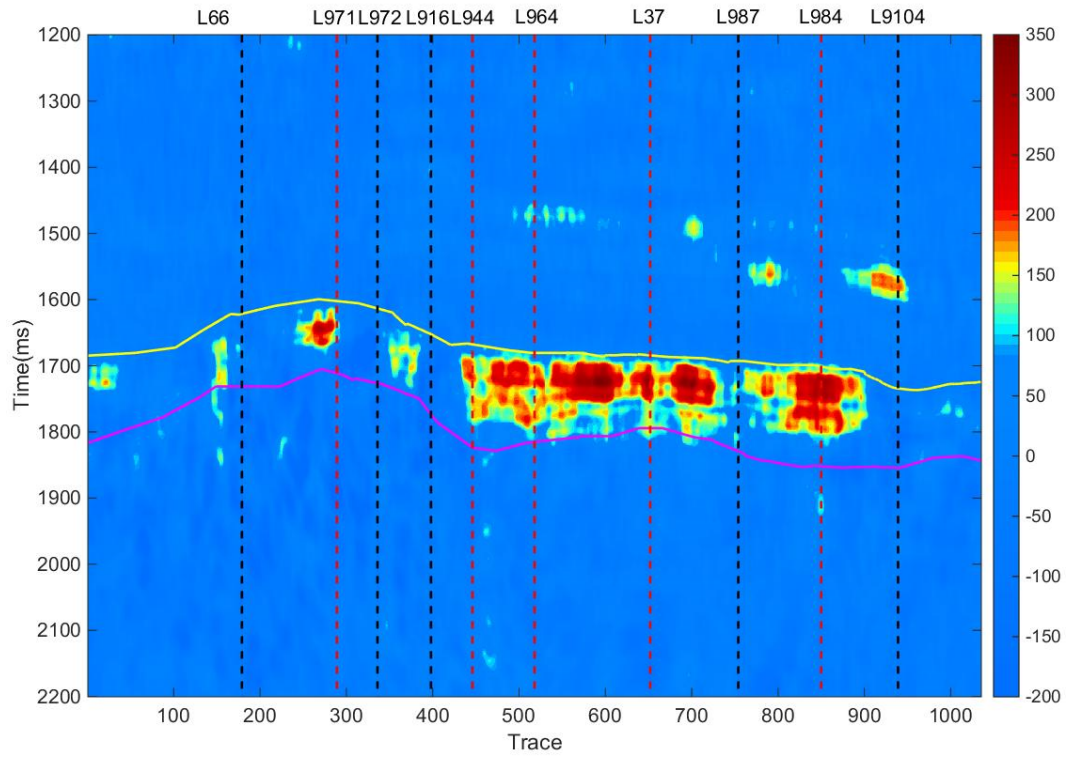
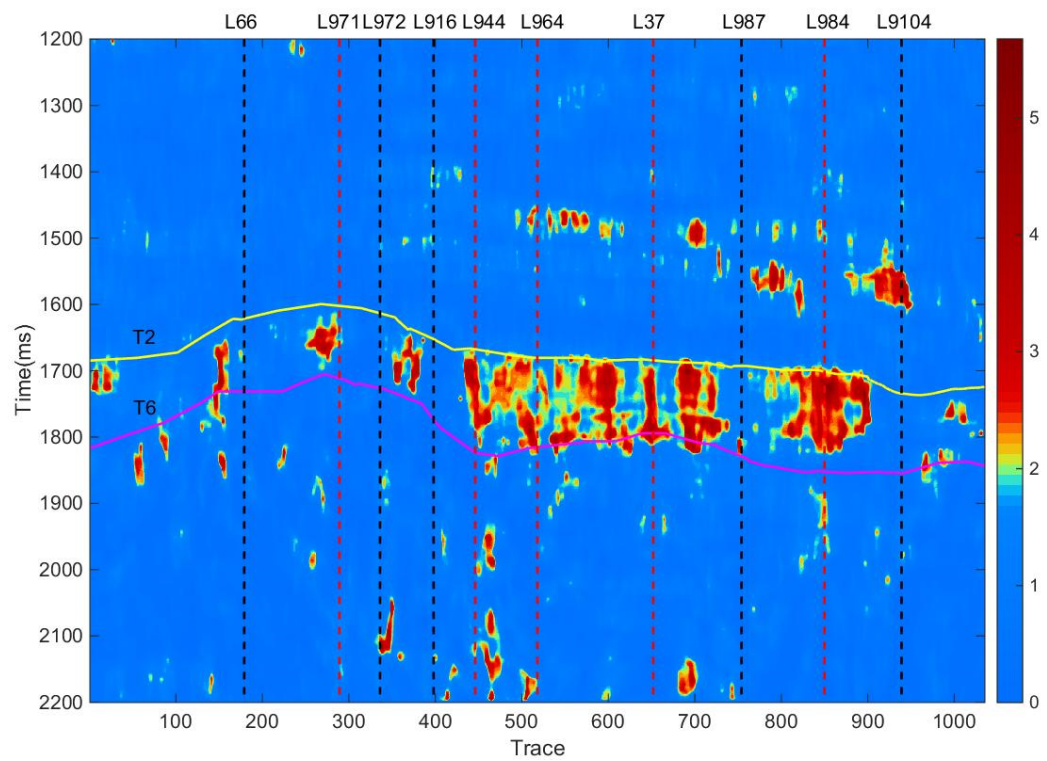


Fig. 18 The energy difference (a) and energy ratio (b) attribute profiles across the water well L66, T2 and T6 correspond to the top and bottom interface of fractured reservoir, the colors mean the energy difference (a) and ratio (b) values, the black dotted lines represent the location of the water-saturated well L66.



(a)



(b)

Fig. 20 The energy difference (a) and energy ratio (b) attribute profiles across wells,

T2 and T6 correspond to the top and bottom interface of fractured reservoir, the colors mean the energy difference (a) and ratio (b) values, the red and black dotted lines represent the locations of oil and water wells.